Harnessing Electronic Structure Modulation of Cu^{2+}-Mediated Layered Double Hydroxide Towards Selective C_2 Pathway in CO_2 Reduction and Plastic Upcycling

Jian Yiing Loh[a,b], Feng Ming Yap[a,b], Elton Song-Zhe Mah[a,b], Xianhai Zeng[c], and Wee-Jun Ong[a,,b,d,e,f,g]*

[a] School of Energy and Chemical Engineering, Xiamen University Malaysia, Selangor Darul Ehsan 43900, Malaysia.

[b] Center of Excellence for NaNo Energy & Catalysis Technology (CONNECT), Xiamen University Malaysia, Selangor Darul Ehsan 43900, Malaysia.

[c] College of Energy, State Key Laboratory of Physical Chemistry of Solid Surfaces, Xiamen University, Xiamen 361102, China.

[d] State Key Laboratory of Physical Chemistry of Solid Surfaces, College of Chemistry and Chemical Engineering, Xiamen University, Xiamen 361005, China.

[e] Gulei Innovation Institute, Xiamen University, Zhangzhou 363200, China.

[f] Shenzhen Research Institute of Xiamen University, Shenzhen 518057, China.

[g] Department of Chemical and Biological Engineering, College of Engineering, Korea University, 145 Anam-ro, Seongbuk-gu, Seoul, 02841 Republic of Korea.

*Corresponding author.

E-mail address: weejun.ong@xmu.edu.my

Electronic Supplementary Information

Calculation of Faradaic Efficiency (FE) Gas Product Analysis

The FE of gaseous products including hydrogen (H_2), carbon monoxide (CO), methane (CH_4), ethane (C_2H_6), and ethylene (C_2H_4), was assessed through the following equation:

$$FE_{gas} = \frac{n \times F \times C \times G \times P}{R \times T \times I_{total}} \times 100\% \quad (1)$$

n = Number of electron transferred during product formation from CO_2 (e.g. CO = 2, CH_4 = 4, H_2 = 2 and C_2H_6 = 12)

F = Faraday Constant (96485 C•mol^{-1})

C = Concentration of gas products determined from GC

G = Gas flow rate ($mL \cdot min^{-1}$)

I = Steady-state cell current density

P = Pressure (1.01×10^5 Pa)

R = Universal gas constant ($8.314\ J \cdot mol^{-1} \cdot K^{-1}$)

T = Temperature (K)

The concentration of gas products was determined from Gas Chromatography (GC). The TCD detector was used for quantification of H_2, while the FID was employed for the detection of CH_4, C_2H_4 and C_2H_6.

Example calculation for specific products:

Example: the GC concentration for H_2 is 2.54×10^{-8}ppm

$$FE_{H2}(\%) = \frac{2 \times 96485 \times 2.54 \times 10^{-8} \times 1.02 \times 10^5}{8.314 \times 293.15 \times 100} = 0.0025$$

$$FE_{H2}(\%) = \frac{0.0025}{FE_{total}} \times 100 = 2.99\%$$

Liquid Product Analysis

The liquid products comprising methanol (CH_3OH) and ethanol (CH_5OH), were determined using a Refractive Index Detector (RID). While other liquid products formate (HCOOH), acetic

acid (CH_2COOH), oxalic acid ($(COOH)_2$), glycolic acid ($HOCH_2COOH$) were analyzed using a diode array detector (DAD). The liquid products were determined with an injection volume of 10 µL at 40 °C. The FE was identified by the following equation:

$$FE_{liquid} = \frac{n \times F \times mol\ of\ product\ formed}{Q_{total}} \times 100\%$$

In the given equation, 'n' represents the number of electrons in the formation of products, F is the Faradaic constant (96845 C mol^{-1}) and Q_{total} represents the total charge passed during the analysis.

PET Oxidation Conversion, Yield and Selectivity

For PET oxidation the concentration of the products were obtained over an hour reaction period. The liquid products were analyzed using an Agilent 1260 Infinity II high-performance liquid chromatography (HPLC) system, equipped with an Agilent HiPlex-H column.

$$Conversion\ (\%) = \frac{n\ (reacted\ reactants)}{n\ (initial)} \times 100\%$$

$$Yield\ (\%) = \frac{n\ (products\ production)}{n\ (initial\ reactants)} \times 100\%$$

Applied bias photo-to-current efficiencies (APBE)

$$\mathrm{ABPEs} = \frac{\mathrm{I} \times (1.23 - \mathrm{V_b}) \times n_F}{\mathrm{P}} \times 100\% \qquad (2)$$

The applied bias photon-to-current efficiencies of photoanode were calculated by using 100% Faradaic efficiency using the above equation. Where I is the photocurrent density (mA cm^{-2}), V_b is the applied bias potential (V_{RHE}), n_F is the faradaic efficiency of the products and P is the incident light power density (AM 1.5G, 100 mW cm^{-2}). The bias potential is external voltage source from the solar panel.

Solar-To-Fuel Conversion Efficiency Calculation (n_{STF})

The energy content of a fuel is defined by its standard molar enthalpy of combustion at 25 °C. The input energy of the system, represented by the power of the light source, can be directly measured using a multimeter and was found to be 96.2 mW/cm^2 (or 0.0962 W). The term fuel refers to the concentration of products, determined via GC/HPLC analysis (in mol). The solar-

to-fuel (STF) conversion efficiency is then calculated as the ratio of the fuel's energy output to the input energy, providing a precise metric of the system's overall performance.

$$n_{STF} = \frac{\text{Standard molar enthalpies of combustion } \left(\frac{\text{kJ}}{\text{mol}}\right) \times Fuel\ (mol)}{Illumination\ power\ (W) \times Operation\ time\ (s)} \quad (3)$$

Standard Molar Enthalpies of Combustion (ΔH_c°)

Products	Chemical Equation	ΔH_c° (kJ/mol)
Hydrogen (H_2)	$H_2(g) + 0.5\ O_2(g) \rightarrow H_2O(l)$	-285.8
Carbon Monoxide (CO)	$CO(g) + 0.5\ O_2(g) \rightarrow CO_2(g)$	-283.0
Methane (CH_4)	$CH_4(g) + 2\ O_2(g) \rightarrow CO_2(g) + 2\ H_2O(l)$	-890.3
Ethylene (C_2H_4)	$C_2H_4(g) + 3\ O_2(g) \rightarrow 2\ CO_2(g) + 2\ H_2O(l)$	-1411.1
Ethane (C_2H_6)	$C_2H_6(g) + 3.5\ O_2(g) \rightarrow 2\ CO_2(g) + 3\ H_2O(l)$	-1560.0
Formic Acid (HCOOH)	$HCOOH(l) + 1.5\ O_2(g) \rightarrow CO_2(g) + 2\ H_2O(l)$	-871.0
Acetic Acid (CH_3COOH)	$CH_3COOH(l) + 2.5\ O_2(g) \rightarrow 2\ CO_2(g) + 3\ H_2O(l)$	-875.0
Methanol (CH_3OH)	$CH_3OH(l) + 1.5\ O_2(g) \rightarrow CO_2(g) + 2\ H_2O(l)$	-726.0
Ethanol (C_2H_5OH)	$C_2H_5OH(l) + 3\ O_2(g) \rightarrow 2CO_2(g) + 3\ H_2O(l)$	-1368.0
Oxalic Acid ($H_2C_2O_4$)	$H_2C_2O_4 + 1.5\ O_2 \rightarrow 2CO_2 + H_2O$	-251.9
Glycolic Acid ($HOCH_2COOH$)	$HOCH_2COOH(l) + 2O_2(g) \rightarrow 2CO_2(g) + 2H_2O(g)$	-4177.8

The standard molar enthalpies of combustion (ΔH_c°) of each component is calculated based on the room temperature.

Full cell energy efficiency

The full-cell energy efficiency for CO_2RR products was calculated by following equation [1, 2]:

$$EE = \frac{(1.23 + (-E_A^0))}{-E_{cell}} \times FE_{product} \times 100\% \quad (4)$$

Where E^0_A is the thermodynamic potential of CO_2 to the specific product. $E^0_{ethanol} = 0.081$ [3]. FE is the faradaic efficiency for the products. E_{cell} is the applied cell voltage in the flow cell system.

**For reliable comparison and accurate evaluation of the overall cell potential, the anodic process was referenced to the standard thermodynamic potential of the OER, since the standard potential for the POR has not been systematically benchmarked in the literature.*

Production cost

Energy consumption was calculated based on 24 h of operation to estimate the energy required for producing 1 tonne of ethanol, assuming an electricity cost of \$0.03 kWh^{-1}. The calculation follows the equation below[4]:

$$Production\ cost\ \left(\frac{\$}{ton_{EtOH}}\right) = \frac{Power\ consumption\ (kW) \times 24\ h \times electricity\ price\ \left(\frac{\$}{kW\ h^{-1}}\right)}{Ethanol\ production\ (ton\ day^{-1})} \quad (5)$$

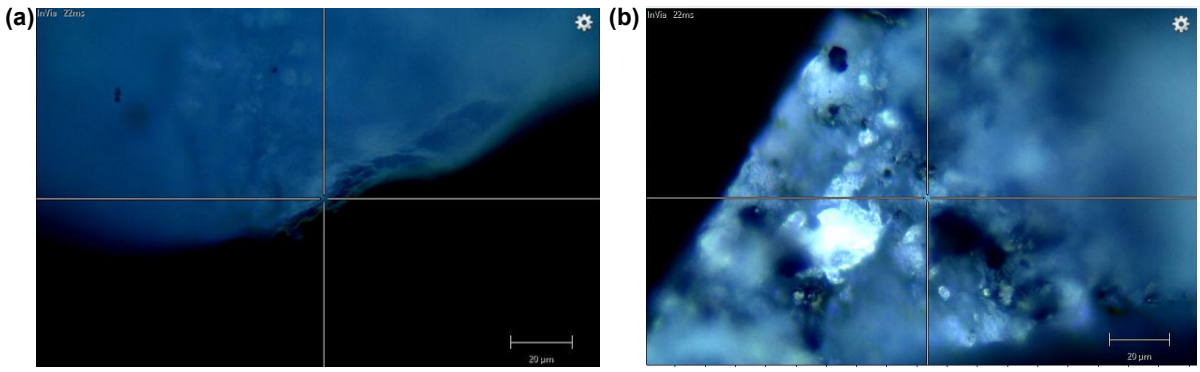


Fig. S1 Raman images of (a) CMA -0.1 and (b) CMA-0.1-G.

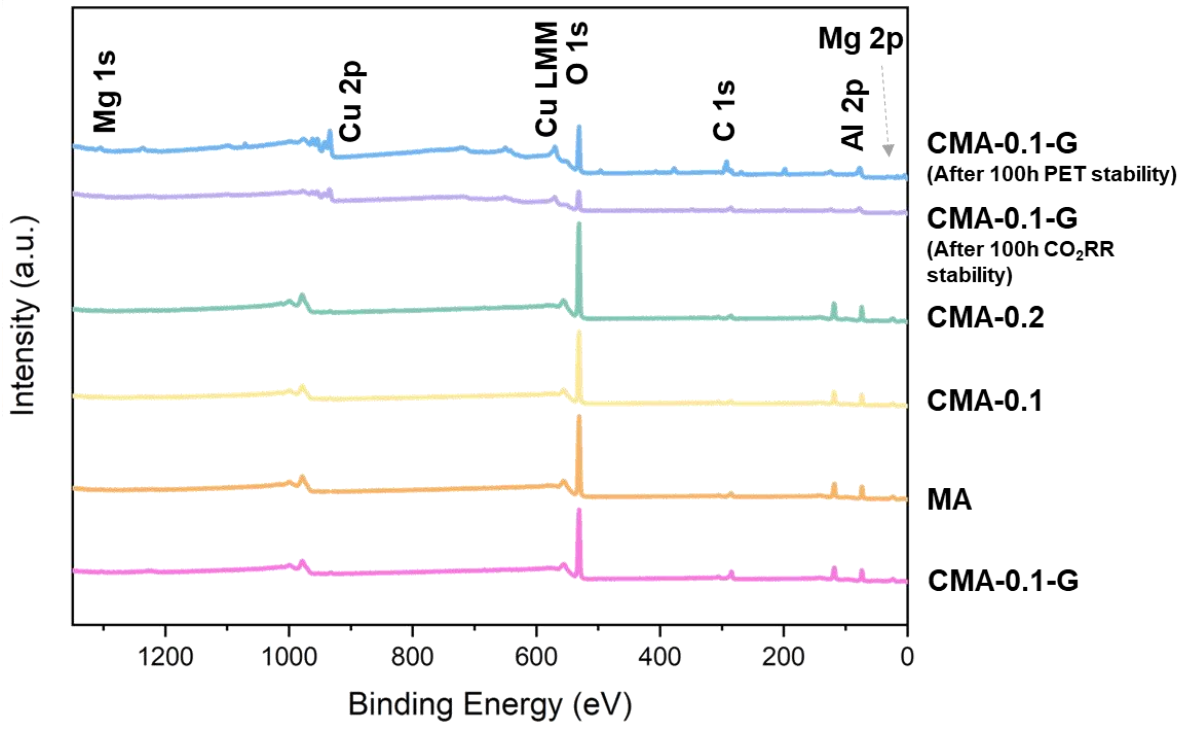


Fig. S2 XPS survey spectra of CuMgAl-LDHs.

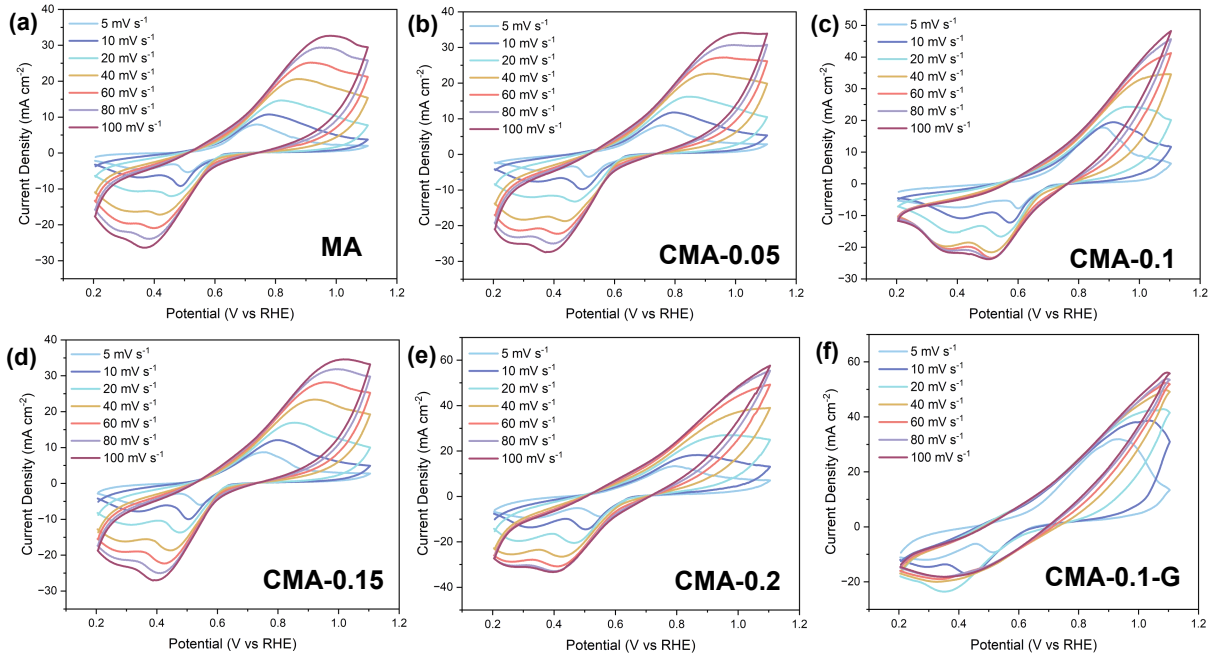


Fig. S3 Electrocatalytic CO_2RR performance evaluation: (a-f) Cyclic voltammetry curves of the as-prepared catalysts.

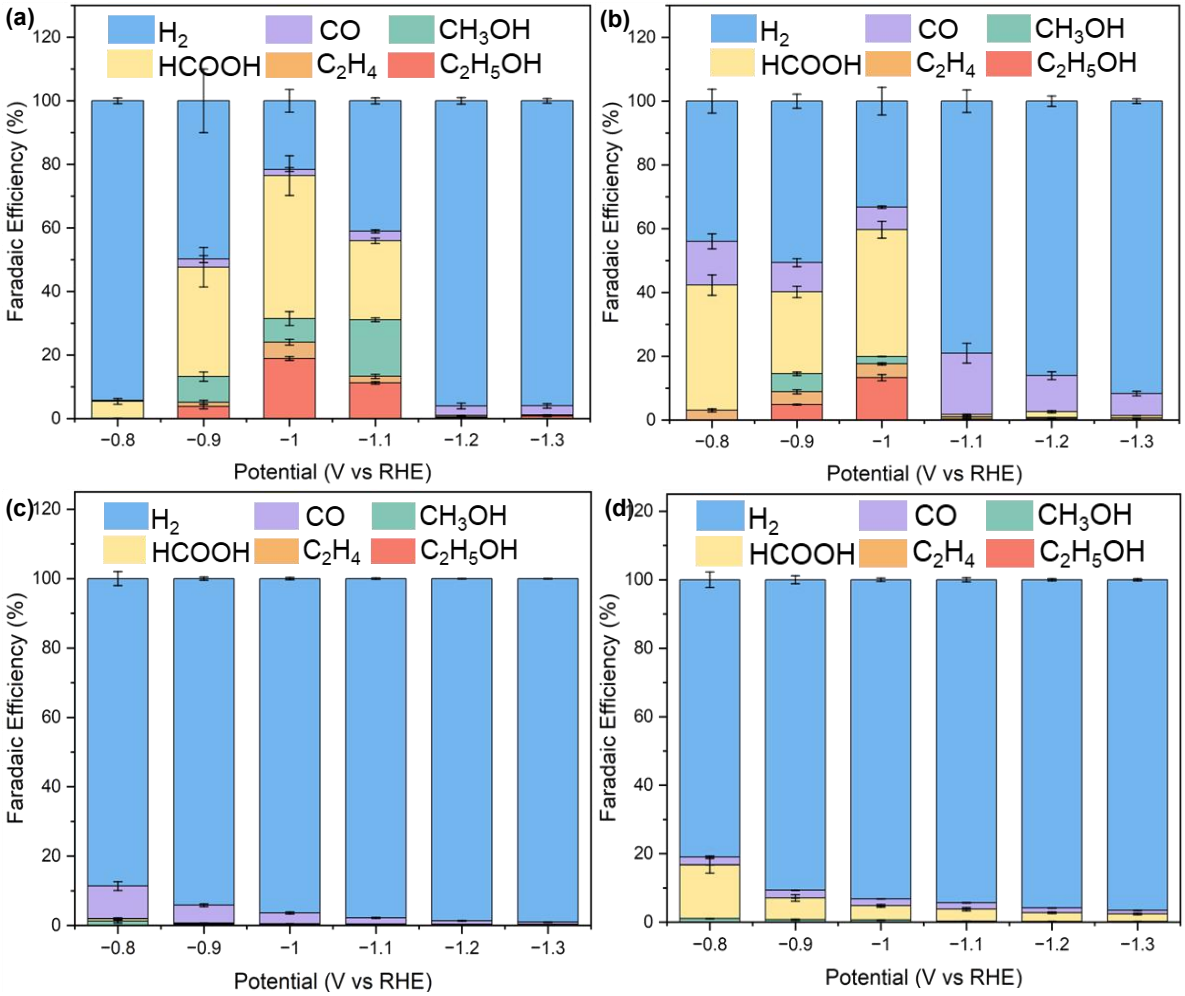


Fig. S4 Electrocatalytic CO_2RR Faradaic Efficiency (FE) (a) CMA-0.1, (b) MA, (c) CuMg-LDH and (d) CuAl-LDH.

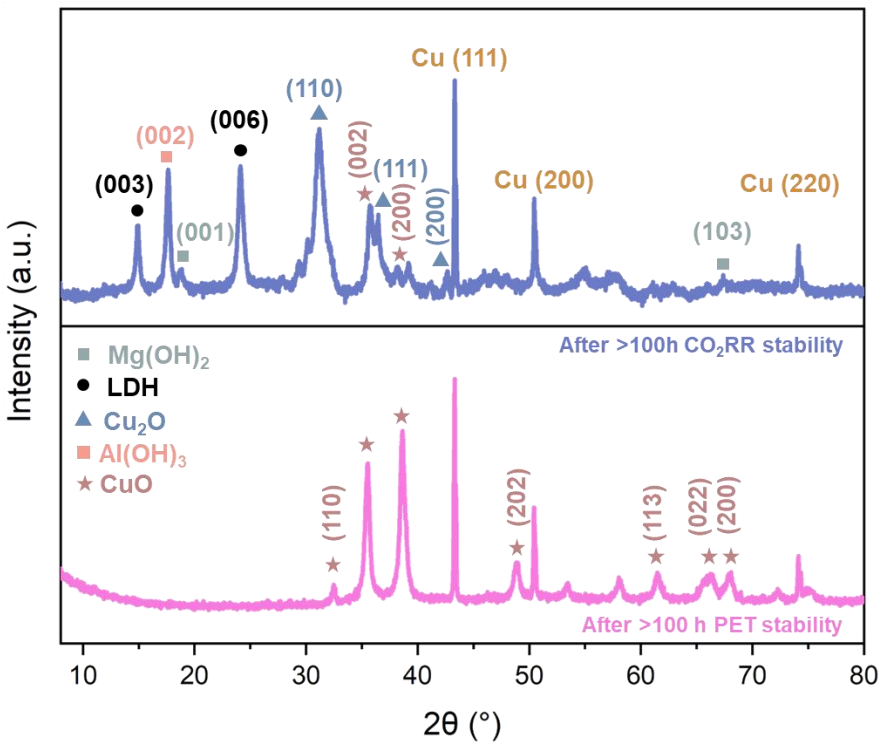


Fig. S5 XRD patterns of CMA-0.1-G after > 100 h stability test for CO_2RR and POR.

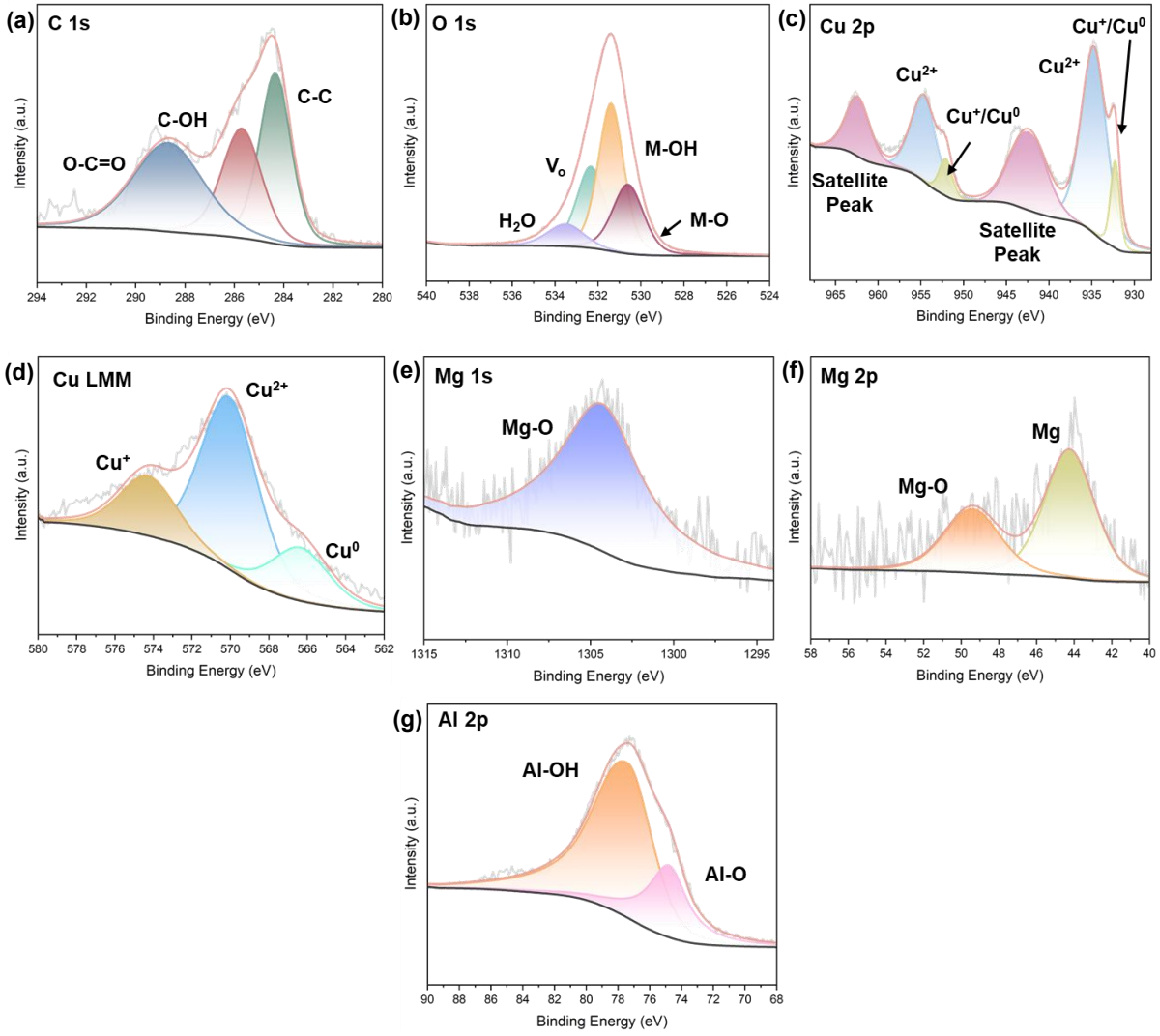


Fig. S6 XPS spectra of CMA-0.1-G after 100 h stability test for CO_2RR: (a) C 1s, (b) O 1s, (c) Cu 2p, (d) Cu LMM, (e) Mg 1s, (f) Mg 2p, (g) Al 2p.

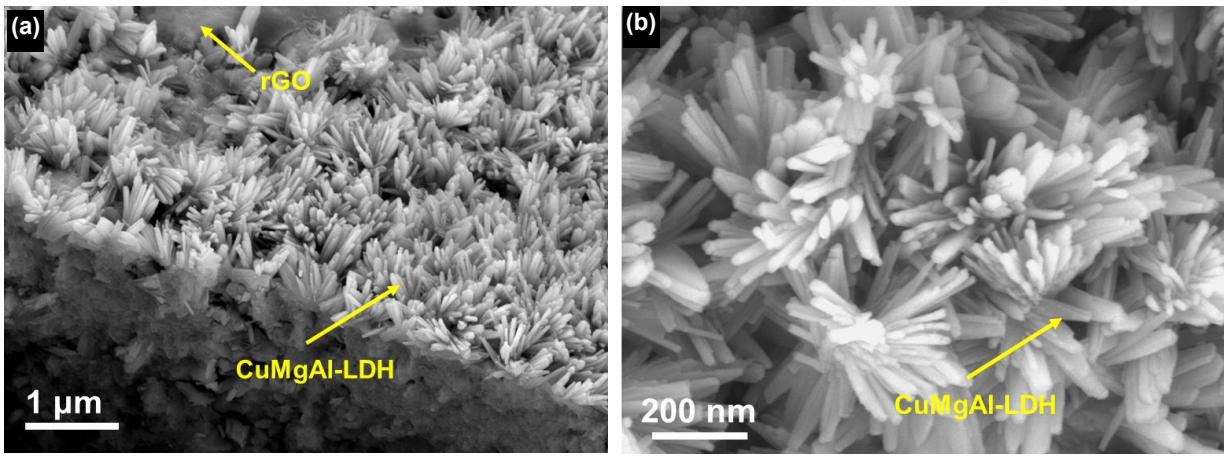


Fig. S7 FESEM images of CMA-0.1-G after 100 h stability test for CO_2RR.

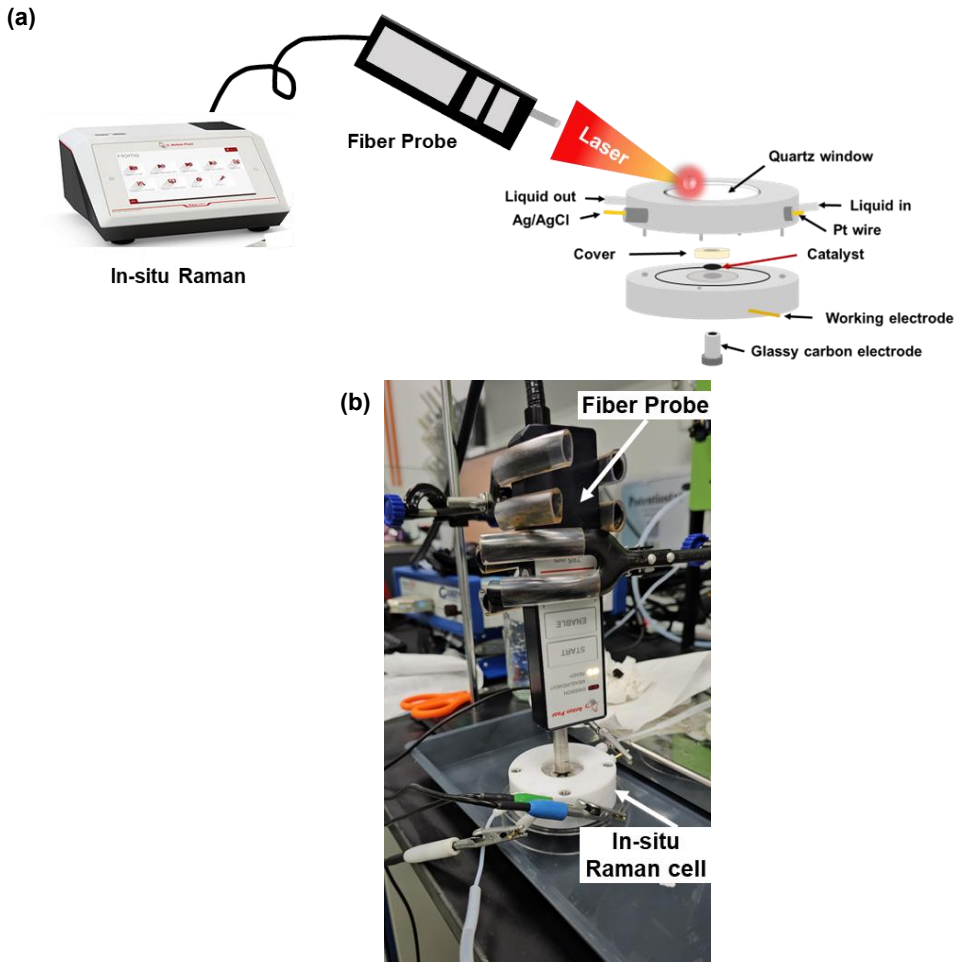


Fig. S8 Photographic representation of in-situ Raman analysis.

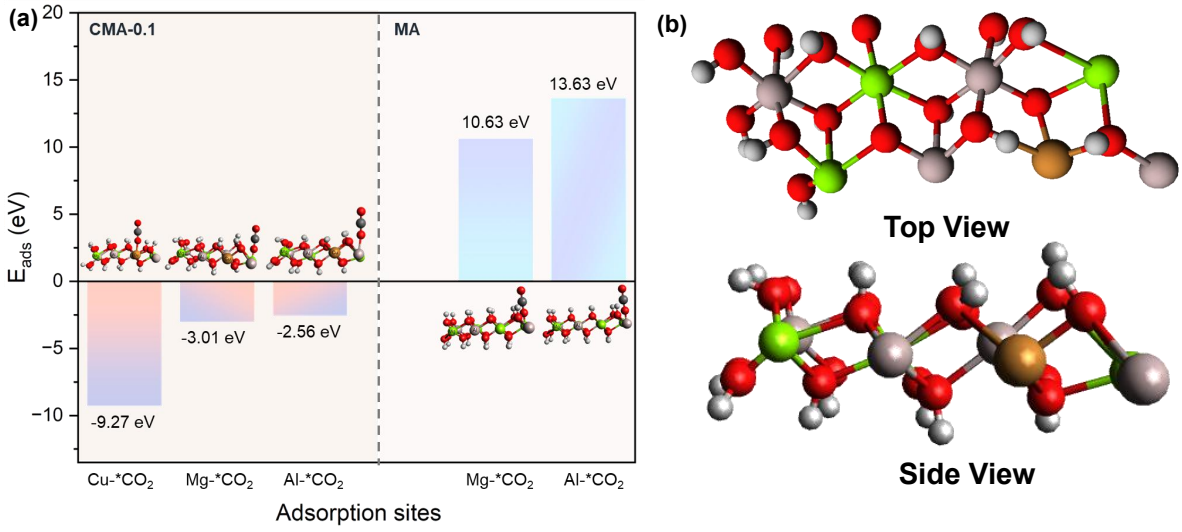


Fig. S9 (a) Adsorption energy of *CO_2 reactant on Cu*, Mg* and Al* for CMA-0.1 and Mg* and *Al on MA. (b) Single unit cell structure of CMA-0.1 (top view and side view) for computational analysis.

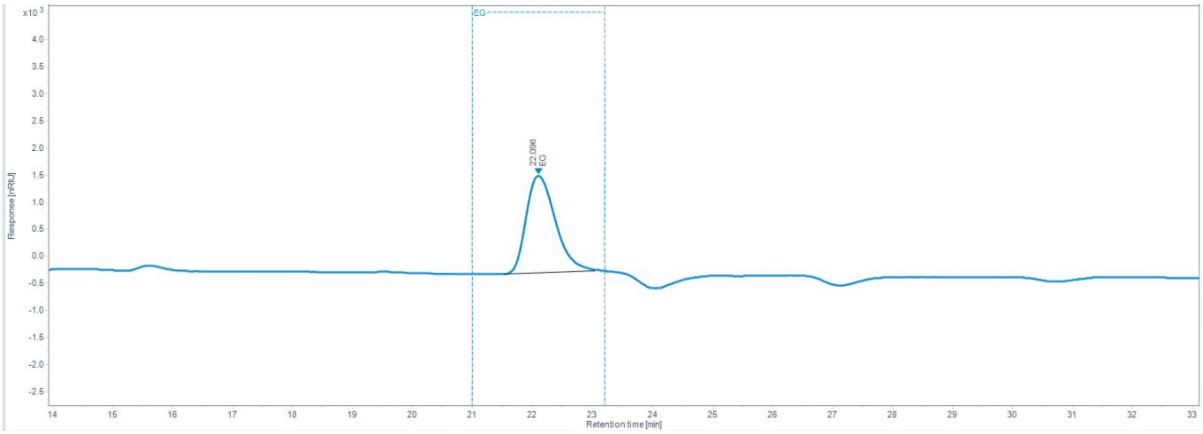


Fig. S10 Raw HPLC chromatogram of PET hydrolysate.

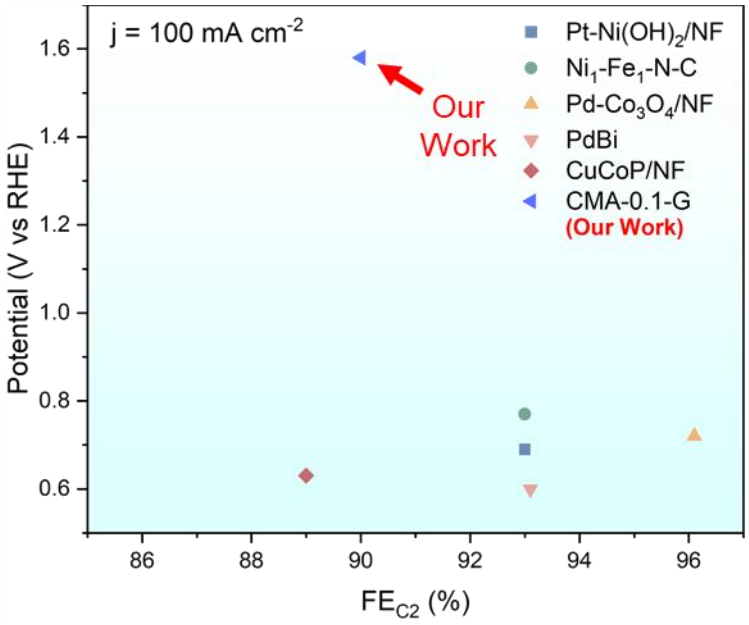


Fig. S11 Comparison plot of typical PET oxidation to produce C_2 products(e.g. Pt-Ni(OH)$_2$/NF [5], Ni$_1$-Fe$_1$-N-C[6], Pd-Co$_3$O$_4$/NF[7], PdBi [8] and CuCoP/NF[9]).

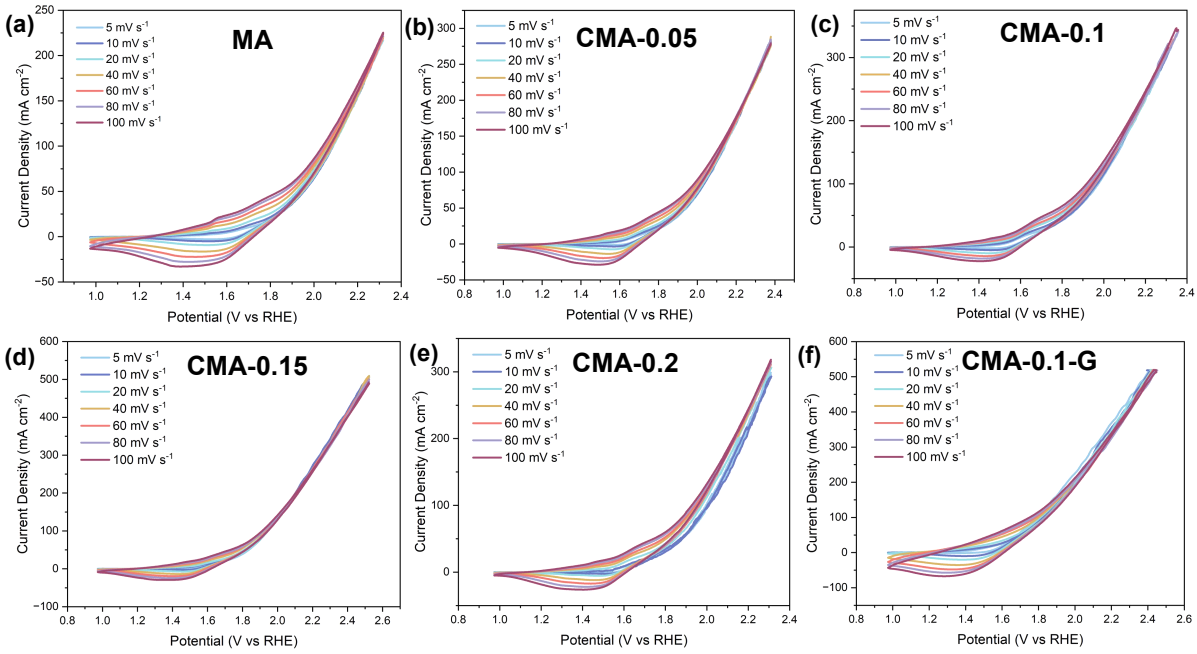


Fig. S12 Electrocatalytic PET oxidation performance evaluation cyclic voltammetry curves of the as-prepared catalysts.

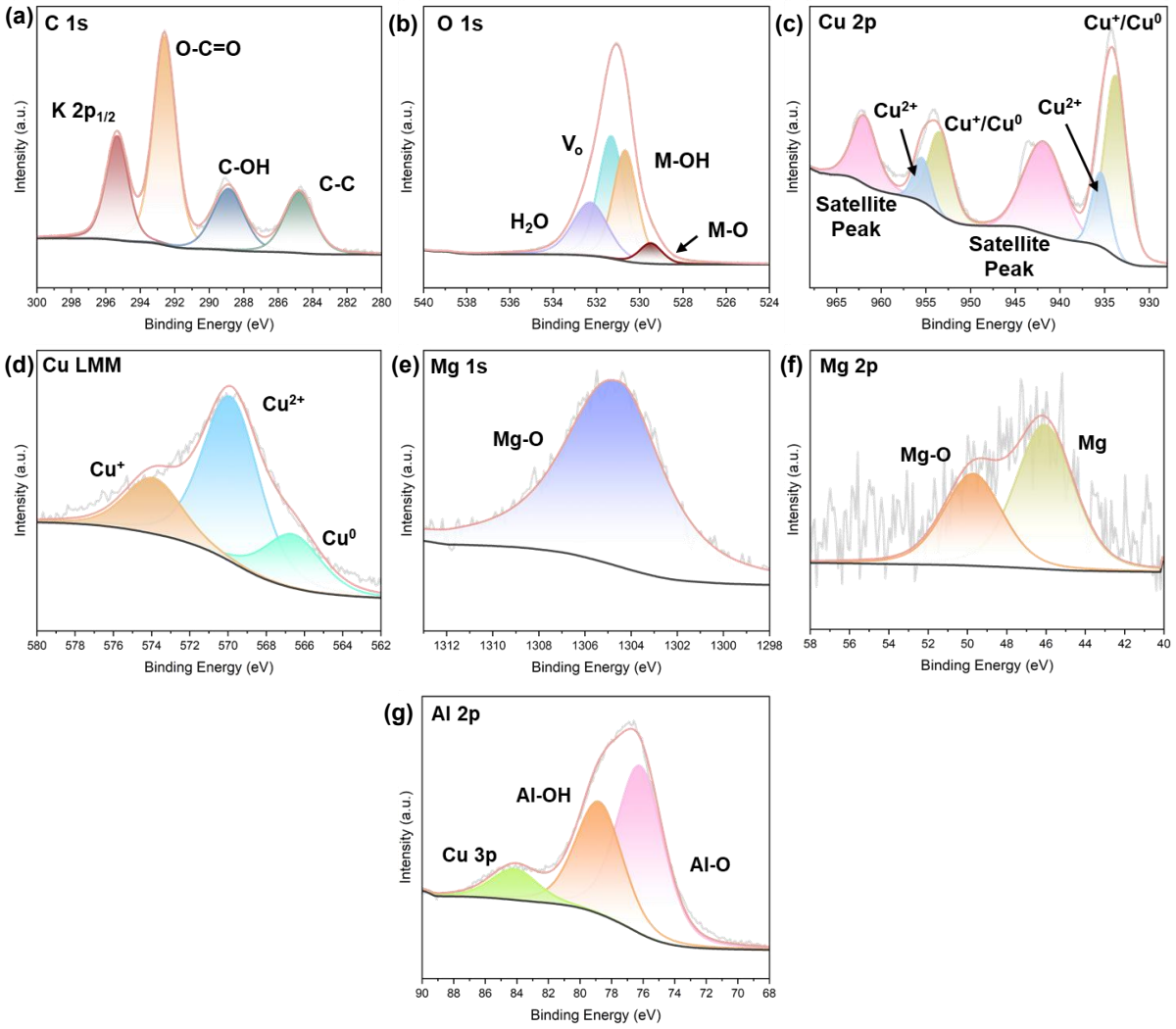


Fig. S13 XPS spectra of CMA-0.1-G after 100 h stability test for PET oxidation: (a) C 1s, (b) O 1s, (c) Cu 2p, (d) Cu LMM, (e) Mg 1s, (f) Mg 2p, (g) Al 2p.

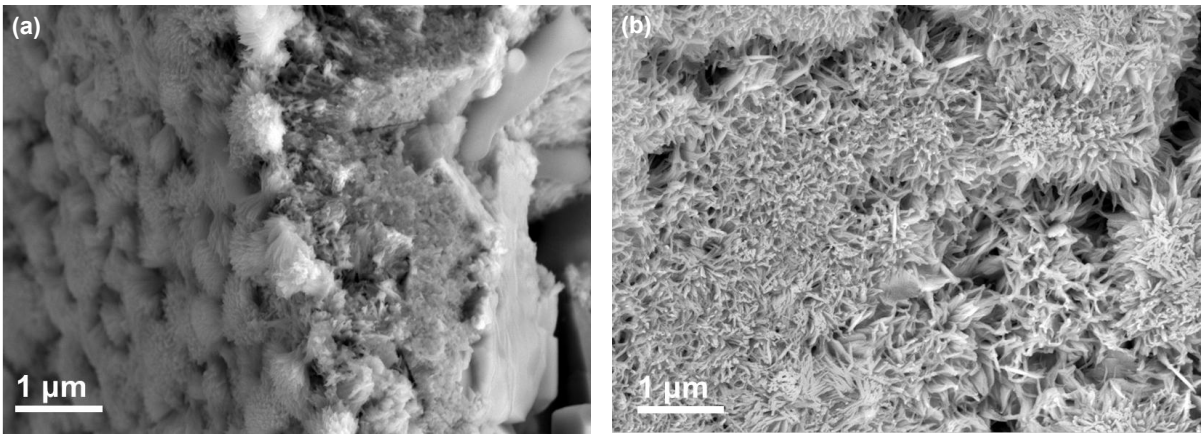


Fig. S14 FESEM analysis of CMA-0.1-G after 100 h stability test for PET oxidation.

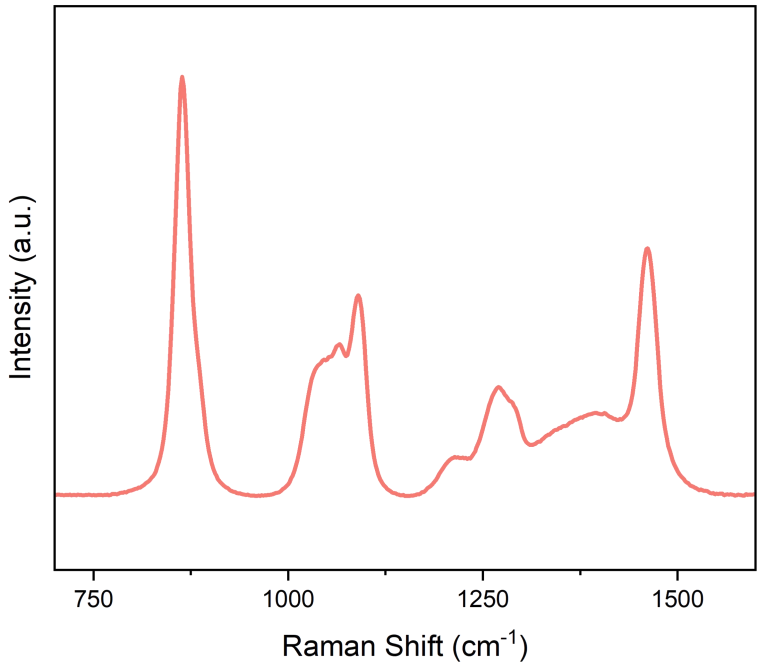


Fig. S15 Raman spectrum for ethylene glycol (EG).

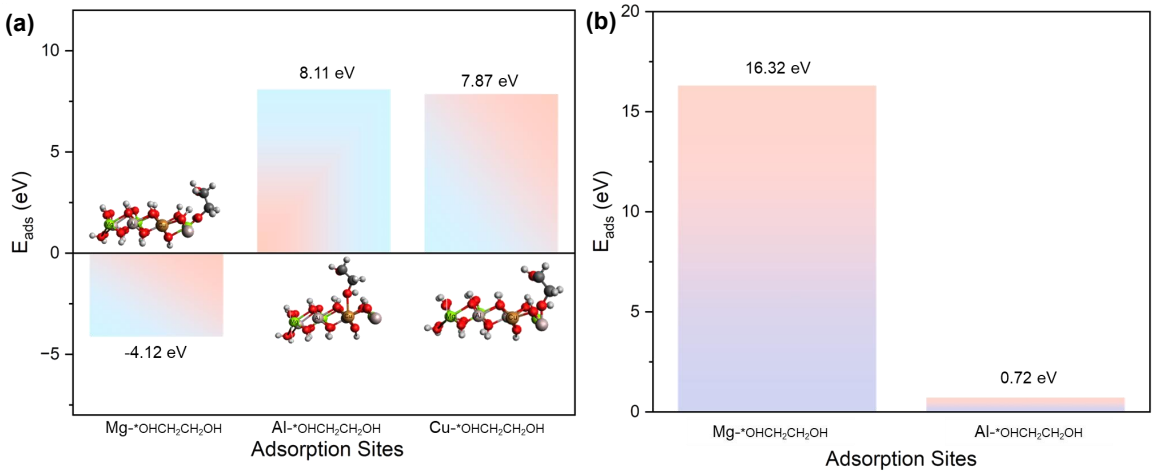


Fig. S16 Comparative adsorption energies of *$OHCH_2CH_2OH$ reactant for (a) CMA-0.1 on Cu*, Mg* and Al* sites and (b) MA on Mg* and Al*during PET oxidation processes.

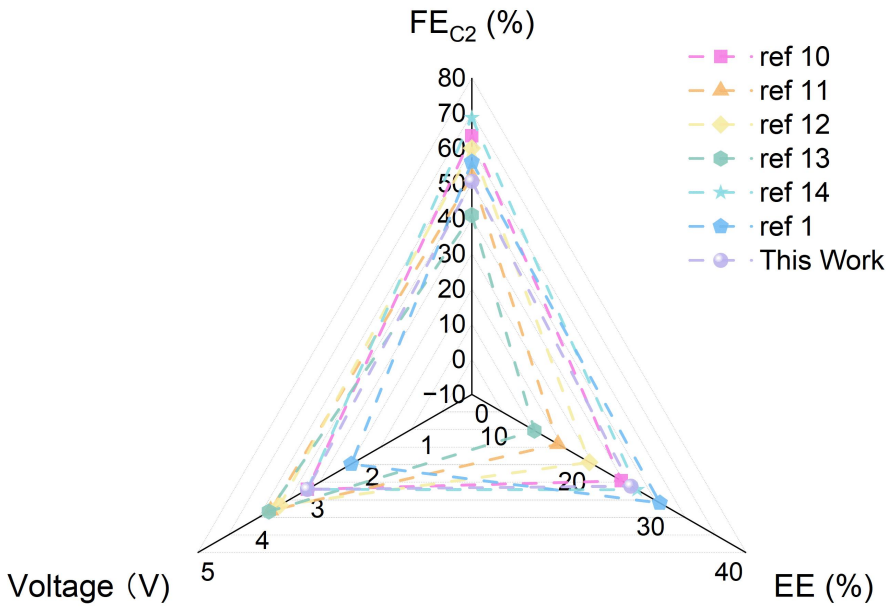


Fig. S17 Comparison graph for energy efficiency and voltage for ethanol. $SnSe/SnSe_2$ [10], Cu-N-C [11], $Cu\text{-}_{DS}$ [12], Cu porphyrin-based metallic complexes [13], Ag^{+}-doped InSe [14], Cu-3 [1].



Fig. S18 Solar-powered integrated two-electrode electrolyzer with natural sunlight outdoor. Experiment details: 5 March 2025; Xiamen University Malaysia, Sepang, morning 10 am."

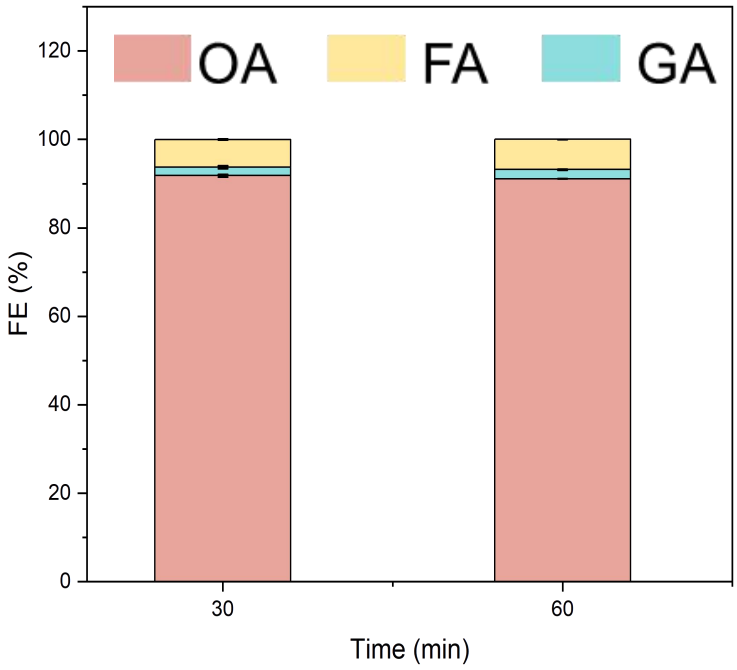


Fig. S19 The Faradaic Efficiency of CMA-0.1-G of the natural sunlight test at the 60th minutes illumination powered H-cell setup.

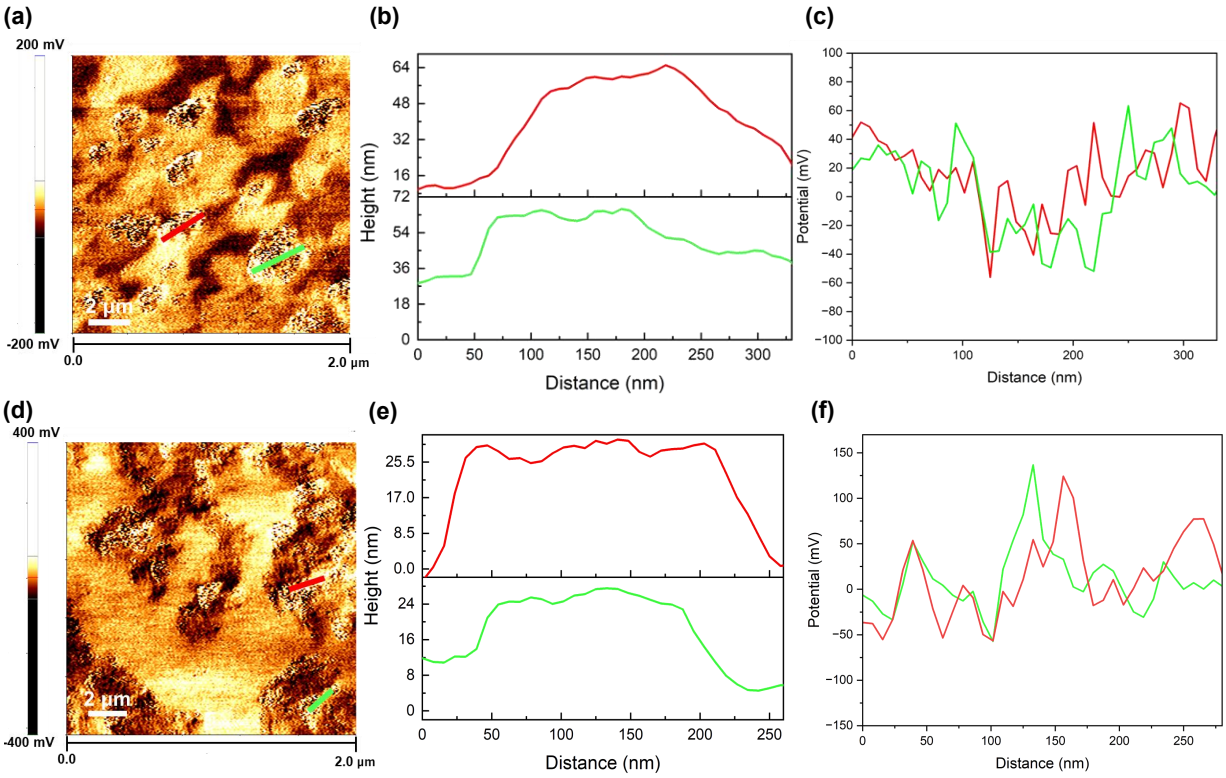


Fig. S20 CMA -0.1 (a) KPFM potential map, (b) height curves, (c) potential graphs. CMA-0.1-G (d) KPFM potential map, (e) height curves, (f) potential graphs.

Tables

Table S1 Summary of XPS CuLMM atomic %

Catalyst	Normalized atomic %		
	Cu+	Cu2+	Cu^0
CMA-0.1	42.86	21.43	35.71
CMA-0.2	30.77	38.46	30.77
CMA-0.1-G	27.78	50.00	22.22

Table S2 Summary of EIS resistance for electrochemical CO_2RR

Sample	Cu:Al molar ratio	
	Theoretical	ICP-MS
CMA-0.05	0.05:0.95	0.041:0.93
CMA-0.1	0.1:0.9	0.09:0.9

Table S3 Summary of EIS resistance for electrochemical CO_2RR

Catalyst	**R_{ct} (Ω)**
MA	296.90
CMA-0.05	76.03
CMA-0.1	53.48
CMA-0.15	120.27
CMA-0.2	130.86
CMA-0.1-G	28.71

Table S4 Comparison table for carbon dioxide reduction (CO_2RR)

Carbon Dioxide Reduction (CO_2RR)							
No	Catalysts	Electrolyte (cell)	RE	CO_2 flowrate (mL min^{-1})	FE (@Potential/ Current density)	Stability	Ref
1	CuMgAl-LDH	1 M KOH (flow-cell)	Hg/HgO	30	FE_{C2+} = 54.96% @ -300 mA cm^{-2}		[15]
2	CuMgAl LDH/CP	0.3 M $KHCO_3$ (H-cell)	Ag/AgCl	20	$FE_{CH3COOH}$ = 84% @ -0.4 V vs RHE	24 h	[16]
3	MgAl-LDH/Cu	1 M $KHCO_3$ (Three-electrode system)	Ag/AgCl	20	FE_{C2H4} = 55.1% @ 300 mA cm^{-2}	7 h	[17]
4	Cu NPs	0.5 M KOH (flow-cell)	Ag/AgCl	100	FE_{CH4} = >70% @ 200 mA cm^{-2}	10 h	[18]
5	CuNiAl-LDHs	0.1 M $KHCO_3$ (H-cell)	Ag/AgCl	N/A	FE_{CH3OH} = 76.4 % @ -1.2 V vs RHE	24 h	[19]

6	Cd-Mg-Al-LDHs@RGO	0.1 M $KHCO_3$ (H-cell)	Ag/AgCl	20	FE_{CO} = 91.5% @ -1.1 V vs RHE	7.5 h (-1.2 V vs RHE)	[20]
7.	Cu-Al/LDHs	1 M $KHCO_3$ (H-cell)	Ag/AgCl	10	FE_{CO} = 42% @ 50 mA	10 h (FE decreased by 5%)	[21]
8.	Ni/Cu	0.1 M KHCO3 (H-cell)	Ag/AgCl	20	FE_{C2} = 42% (-0.86V vs. RHE)	6 h with FE C_2 of ~25%	[22]
9.	S-doped Cu (Cu S 811)	0.1 M $KHCO_3$ (H-cell)	Ag/AgCl	N/A	$FE_{formate}$ = 92% @ -1.0 V vs RHE	48 h (-1.0 V vs RHE)	[23]
10.	Cu-Zn@Al-fum	0.1 M $KHCO_3$ (H-cell)	Ag/AgCl	7.5	FE_{C2} = 12% @-1.0 V vs RHE	4 h (current density decrease by 10-15%)	[24]
11.	CeO_2-Cu_2O/GA	0.1 M $KHCO_3$ (H-cell)	Ag/AgCl	20	FE_{C2+} > 62% (-0.8 to -1.2 V)	80 h with FE C2+ ~ 62%	[25]
12.	Ag core/porous Cu shell particles	1 M $KHCO_3$ (GDE)	Ag/AgCl	20	FE_{C2+} = 29 % @ -0.65 V vs RHE	1 h	[26]
13.	Ag-Cu_2OPB	0.1 M $KHCO_3$ (H-cell)	Ag/AgCl	40	FE_{C2+} = 43.65% (-0.9 to -1.4 V vs. RHE)	3 h	[27]
14.	Cu-complex/Cu	0.5 M $KHCO_3$	Ag/AgCl	N/A	FE_{C2} = 80% @-0.4 V vs RHE	24 h @ -0.4 V vs RHE	[28]
15.	Cu@Ag-2 NPs	1 M KOH (GDE)	Ag/AgCl	5	FE_{C2} = 67.6% @-1.1 V vs RHE	14 h @-1.1 V vs RHE	[29]
16.	$Cu_{0.9}Ag_{0.1}$	3 M KOH (GDE)	Mini-RHE	15	FE_{C2+} = 63% @-0.4 V vs RHE	-	[30]
17.	Cu Sas/UIO-H_2	0.5 M $KHCO_3$ (H-cell)	Ag/AgCl	100	FE_{C2} = 58.62% @-0.66 V vs RHE	>12 h @-0.66 V vs RHE	[31]
18.	$Cu_{88}Ag_{12}$NW	0.5 M $KHCO_3$ (H-cell)	Ag/AgCl	-	FE_{C2H4} = 77.8% @-1.0V vs RHE	>12 h @ -1.0 V vs RHE	[32]
19.	Cu-N_4/C	0.1 M $KHCO_3$ (H-cell)	Ag/AgCl	-	FE_{C2H5OH} = 53.11% @-0.6 V vs RHE	>16 h @-0.6 V vs RHE	[33]
20.	CMA-0.1-G	0.1 M $KHCO_3$ (H-cell)	Ag/AgCl	20	FE_{C2} = ~52% @ -1 V vs RHE	>100 h @ 50 mA cm^{-2}	This Work

FE = Faradaic Efficiency; PET = Polyethylene Terephthalate; NPs: Nanoparticles; LDH: Layered Double Hydroxides; GDE = Gas diffusion electrpde; CFP = Carbon Fiber Paper; CF = Copper foam

Table S5 Summary of EIS resistance for electrochemical POR.

Catalyst	**R_{ct} (Ω)**
MA	75.06
CMA-0.05	6.50
CMA-0.1	12.43
CMA-0.15	8.75
CMA-0.2	19.84
CMA-0.1-G	3.00

Table S6 Comparison table for polyethylene terephthalate (PET) oxidation

Polyethylene terephthalate oxidation								
No	Catalysts	Potential (vs RHE)	Electrolyte (Cell)	RE	FE of oxidation product	Stability	Cathodic Reaction	Ref
1.	Co-based 1D coordination polymer	1.42 V @ 10 mA cm^{-2}	1 M KOH + 0.1 M EG (Three electrode cell)	Ag/AgCl	$FE_{formate}$ = 77% @ 1.41 V vs RHE	N/A	-	[34]
2.	Pt-Ni$(OH)_2$/NF	0.69 V @ 100 mA cm^{-2}	1 M KOH + 0.1 M EG (Three electrode cell)	Hg/HgO	FE_{GA} = 93% @0.69 V vs RHE	5 h (Current retained @56.8%)	-	[5]
3.	Ru-CoOOH/NF	~1.5 V @ 100 mA cm^{-2}	1 M KOH + PET hydrolysate (H-cell)	Hg/HgO	$FE_{formate}$ = 96.53% @ 1.33 V vs RHE	5 consecutive cycles @ 1.33 V vs RHE	Ru-Co$(OH)_2$ for NO_3RR Bifunctional: 1.71 @ 150 mA cm^{-2}	[35]
4.	PdFe/N-CNT	32 mV @ 10 mA cm^{-2}	1 M KOH + 0.3 M EG (H-cell)	Hg/HgO	$FE_{formate}$ = 87% @ 1.22 V vs RHE	15 h @ 1.2 V vs RHE	HER MEA flow cell: 1.68 V @ 500 mA cm^{-2}	[36]
5.	CuCuO@rGO	1.15 V @ 20 mA cm^{-2}	1 M KOH + PET (H-cell)	Ag/AgCl	$FE_{formate}$ = 85.7% @1.5 V vs RHE	72 h @ 1.4 V vs RHE	Cathodic CO_2RR: BOC@rGO 1.9 V @ 10 mA cm^{-2}	[37]
6.	CoV-LDH	1.47 V @ 250 mA cm^{-2}	PET hydrolysate (Three electrode cell)	Ag/AgCl	FE_{HCOOH} = 91.33 % @ 1.45 V vs RHE	36 h @ 13 mA cm^{-2}	HER Bifunctional MEA flow cell 1.78 V @ 100 mA cm^{-2}	[38]
7.	PdCu/Ni$(OH)_2$	0.69 V @ 500 mA cm^{-2}	3 M KOH +1 M EG (Three electrode cell)	Ag/AgCl	FE_{GA} = 91.7 % @ 2 A cm^{-2}	12 h @ 200 mA cm^{-2}	HER Bifunctional MEA flow cell <2 V @ 1 A cm^{-2}	[39]
8.	$NiCo_2O_4$/CFP	1.25 V @ 50 mA cm^{-2}	1 M NaOH + 0.1 M PET (Three electrode cell)	SCE	FE_{HCOOH} = > 90% @ 1.45 V vs RHE	N/A	Cathodic CO_2RR: 1.9 V @ 20 mA cm^{-2} FE_{HCOOH} = 155 % @ 1.9V vs RHE (bifunctional)	[40]
9.	Pd/NF	-	1 M KOH + EG (H-cell)	Ag/AgCl	FE_{GA} = 96.45 %	~15 h @ 0.93 V vs RHE	-	[41]
10.	$Pd_{67}Ag_{33}$	0.53 V @ 10 mA cm^{-2}	1 M KOH + 1 M EG	Hg/HgO	FE_{GA} = 92.7%	~ 80 h	FE_{HCOOH} = 92.5% @ -	[42]

					@ 1.0 V vs RHE		0.27 V	
11.	Au/NiO	-	1 M KOH + EG (Three electrode cell)	Hg/HgO	FE_{GA} > 94 % @ 250 mA cm^{-2}	120 h	FE_{H2} > 97% @ -250 mA cm^{-2}	[43]
12.	Ni_1-Fe_1-N-C dual single-atom catalysts	0.77 V @ 100 mA cm^{-2}	1 M KOH + 0.1 M EG (H-cell)	Ag/AgCl	FE_{GA} = 96.1% @1.5 V vs RHE	100 h	-	[6]
13.	Pd-Co_3O_4/NF	0.72 V @ 100 mA cm^{-2}	1 M KOH + 1 M EG (H-cell)	Hg/HgO	FE_{GA} = 93.1 % @ 0.9 V vs RHE	-	-	[7]
14.	NiCo-OH	1.33 V @ 100 mA cm^{-2}	1 M KOH + 0.5 M EG (Three-electrode cell)	Hg/HgO	FE_{C2} = 4.2 % @ 1.3 V vs RHE	50 h @ 1.4 V	-	[44]
15.	PdBi	0.6 V @ 100 mA cm_{-2}	1 M KOH + 0.5 M EG (H-cell)	Hg/HgO	FE_{GA} >89% (0.5 V to 1.2 V)	100 h @ 150 mA cm^{-2}	Oxalic acid reduction reaction TIO_2/TP FE_{GA} = 83% @ -0.49 V vs RHE	[8]
16.	CuCoP/NF	0.63 V @ 100 mA cm^{-2}	1 M KOH + 1 M EG (Three-electrode cell)	Hg/HgO	FE_{C2} = 90% @ 0.8 V vs RHE	>40 h @ 0.8 V vs RHE	HER: 117 mV @ -100 mA cm^{-2}	[9]
17.	CMA-0.1-G	~1.58 V @ 100 mA cm^{-2}	1 M KOH + PET hydrolysate (H-cell)	Ag/AgCl	FE_{C2} = 84.6 %	>100 h @ 50 mA cm^{-2}	1.25 V vs RHE @ 10 mA cm^{-2}	This Work

FE = Faradaic Efficiency; PET = Polyethylene Terephthalate; NPs: Nanoparticles; LDH: Layered Double Hydroxides; GDE = Gas diffusion electrpde; CFP = Carbon Fiber Paper; CF = Copper foam; GA = Glycolic acid

Chromatogram Raw Data and Calibration Curve

Table S7 Raw data chromatogram for GC and HPLC (CO_2RR - CMA-0.1-G at -1 V vs RHE)

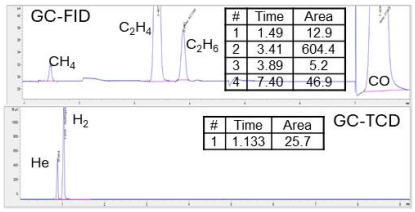
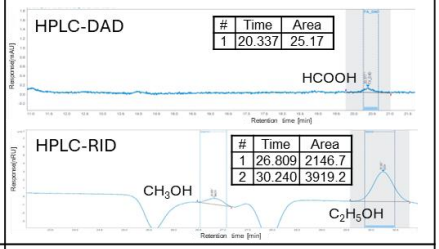
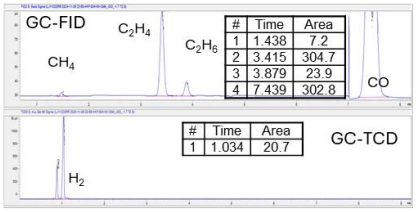
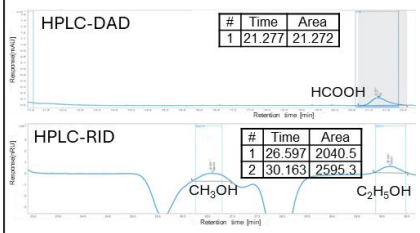
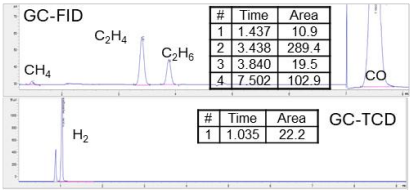
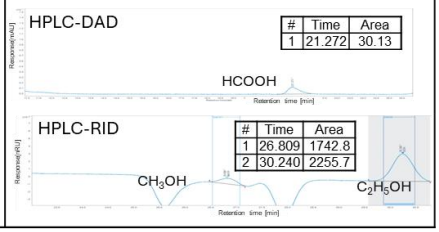
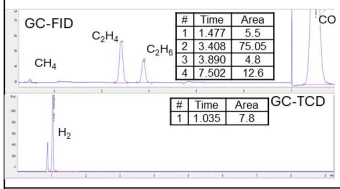
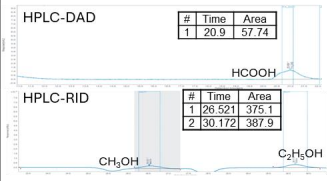
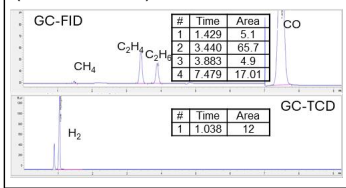
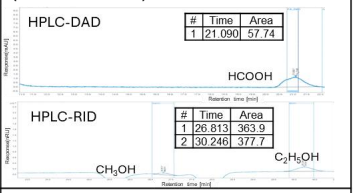
<table>
<tr><th colspan="2">Raw data chromatogram</th></tr>
<tr><td>Gas Chromatography (GC)</td><td>High Performance Liquid Chromatography (HPLC)</td></tr>
<tr><td colspan="2">CMA-0.1-G</td></tr>
<tr><td>CMA-0.1-G (1st Run)
(-1.0 V vs RHE)

</td><td>CMA-0.1-G (1st Run)
(-1.0 V vs RHE)

</td></tr>
<tr><td>CMA-0.1-G (2nd Run)
(-1.0 V vs RHE)

</td><td>CMA-0.1-G (2nd Run)
(-1.0 V vs RHE)

</td></tr>
<tr><td>CMA-0.1-G (3rd Run)3
(-1.0 V vs RHE)

</td><td>CMA-0.1-G (3rd Run)
(-1.0 V vs RHE)

</td></tr>
</table>

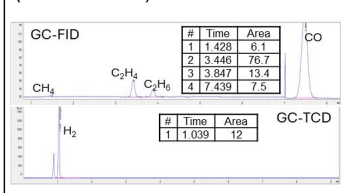
Table S8 Raw data chromatogram for GC and HPLC (CO_2RR - CMA-0.1 at -1 V vs RHE)

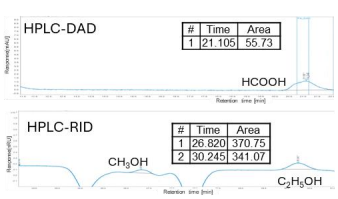
<table>
<tr><th colspan="2">Raw data chromatogram</th></tr>
<tr><td>Gas Chromatography (GC)</td><td>High Performance Liquid Chromatography (HPLC)</td></tr>
<tr><td colspan="2">CMA-0.1-G</td></tr>
<tr><td>CMA-0.1 (1st Run)
(-1.0 V vs RHE)


<table>
<tr><th>#</th><th>Time</th><th>Area</th></tr>
<tr><td>1</td><td>1.477</td><td>5.5</td></tr>
<tr><td>2</td><td>3.408</td><td>75.05</td></tr>
<tr><td>3</td><td>3.890</td><td>4.8</td></tr>
<tr><td>4</td><td>7.502</td><td>12.6</td></tr>
</table>
<table>
<tr><th>#</th><th>Time</th><th>Area</th></tr>
<tr><td>1</td><td>1.035</td><td>7.8</td></tr>
</table></td><td>CMA-0.1 (1st Run)
(-1.0 V vs RHE)


<table>
<tr><th>#</th><th>Time</th><th>Area</th></tr>
<tr><td>1</td><td>20.9</td><td>57.74</td></tr>
</table>
<table>
<tr><th>#</th><th>Time</th><th>Area</th></tr>
<tr><td>1</td><td>26.521</td><td>375.1</td></tr>
<tr><td>2</td><td>30.172</td><td>387.9</td></tr>
</table></td></tr>
<tr><td>CMA-0.1 (2nd Run)
(-1.0 V vs RHE)


<table>
<tr><th>#</th><th>Time</th><th>Area</th></tr>
<tr><td>1</td><td>1.429</td><td>5.1</td></tr>
<tr><td>2</td><td>3.440</td><td>65.7</td></tr>
<tr><td>3</td><td>3.883</td><td>4.9</td></tr>
<tr><td>4</td><td>7.479</td><td>17.01</td></tr>
</table>
<table>
<tr><th>#</th><th>Time</th><th>Area</th></tr>
<tr><td>1</td><td>1.038</td><td>12</td></tr>
</table></td><td>CMA-0.1 (2nd Run)
(-1.0 V vs RHE)


<table>
<tr><th>#</th><th>Time</th><th>Area</th></tr>
<tr><td>1</td><td>21.090</td><td>57.74</td></tr>
</table>
<table>
<tr><th>#</th><th>Time</th><th>Area</th></tr>
<tr><td>1</td><td>26.813</td><td>363.9</td></tr>
<tr><td>2</td><td>30.246</td><td>377.7</td></tr>
</table></td></tr>
<tr><td>CMA-0.1 (3rd Run)
(-1.0 V vs RHE)


<table>
<tr><th>#</th><th>Time</th><th>Area</th></tr>
<tr><td>1</td><td>1.428</td><td>6.1</td></tr>
<tr><td>2</td><td>3.446</td><td>76.7</td></tr>
<tr><td>3</td><td>3.847</td><td>13.4</td></tr>
<tr><td>4</td><td>7.439</td><td>7.5</td></tr>
</table>
<table>
<tr><th>#</th><th>Time</th><th>Area</th></tr>
<tr><td>1</td><td>1.039</td><td>12</td></tr>
</table></td><td>CMA-0.1 (3rd Run)
(-1.0 V vs RHE)


<table>
<tr><th>#</th><th>Time</th><th>Area</th></tr>
<tr><td>1</td><td>21.105</td><td>55.73</td></tr>
</table>
<table>
<tr><th>#</th><th>Time</th><th>Area</th></tr>
<tr><td>1</td><td>26.820</td><td>370.75</td></tr>
<tr><td>2</td><td>30.245</td><td>341.07</td></tr>
</table></td></tr>
</table>

Table S9 Raw data chromatogram for HPLC (POR stability)

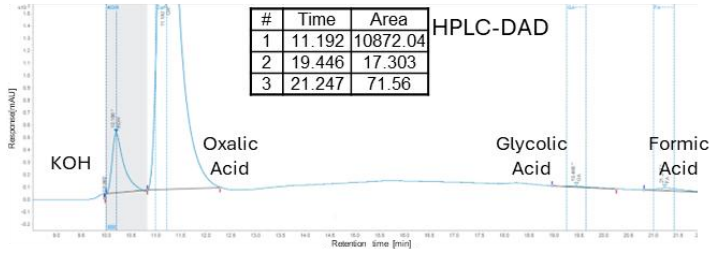
Raw data chromatogram

High Performance Liquid Chromatography (HPLC)

CMA-0.1-G: 48 hours

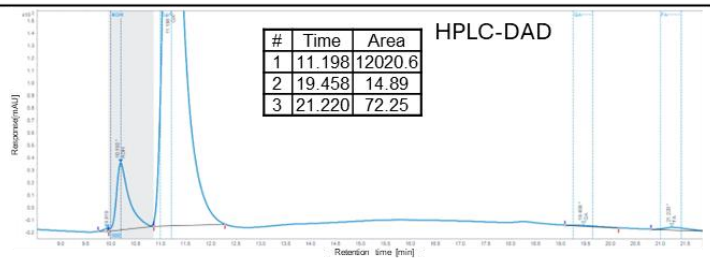
1st Run

#	Time	Area
1	11.192	10872.04
2	19.446	17.303
3	21.247	71.56



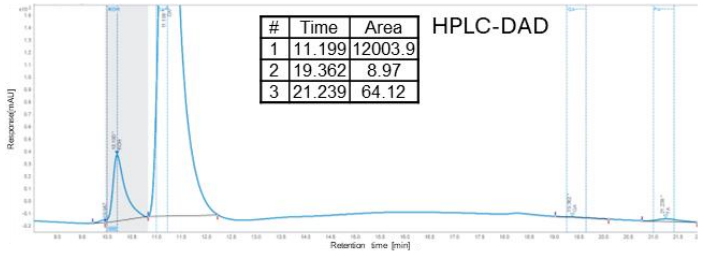
2nd Run

#	Time	Area
1	11.198	12020.6
2	19.458	14.89
3	21.220	72.25



3rd Run

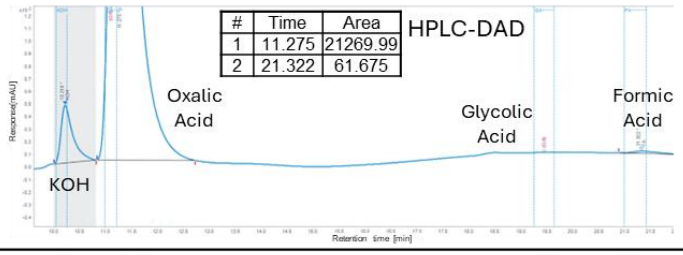
#	Time	Area
1	11.199	12003.9
2	19.362	8.97
3	21.239	64.12



CMA-0.1-G: 100 hours

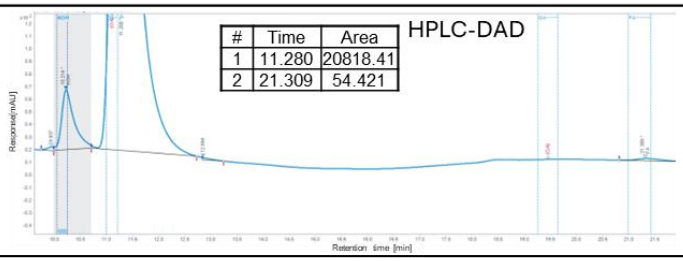
1st Run

#	Time	Area
1	11.275	21269.99
2	21.322	61.675



2nd Run

#	Time	Area
1	11.280	20818.41
2	21.309	54.421



3rd Run

#	Time	Area
1	11.823	20906.31
2	21.347	49.38

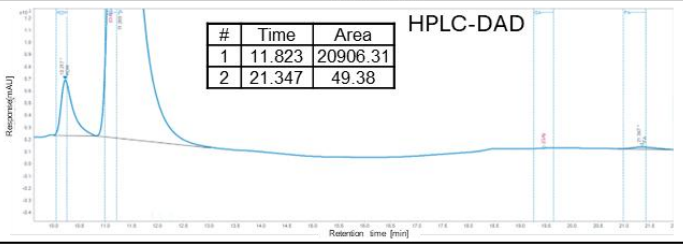


Table S10 Gas Chromatography (GC) calibration curve

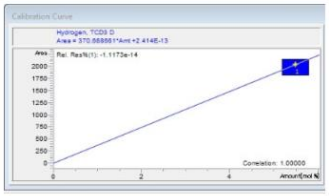
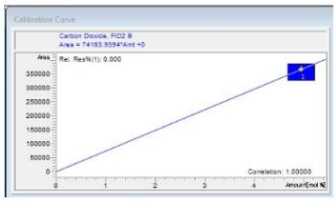
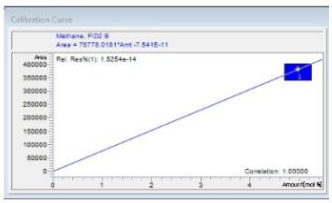
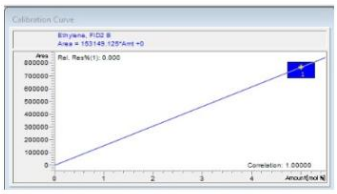
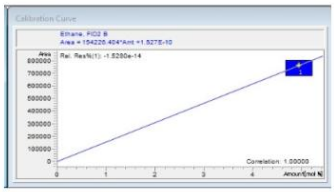
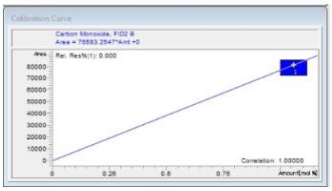
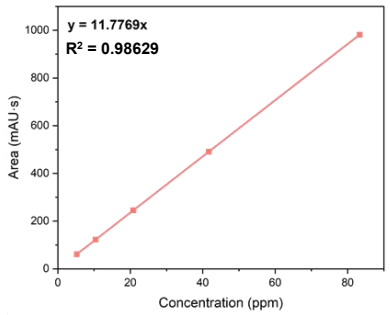
Calibration curve		
Hydrogen, H_2	Carbon dioxide, CO_2	Methane, CH_4
		
Ethylene, C_2H_4	Ethane, C_2H_6	Carbon monoxide, CO
		

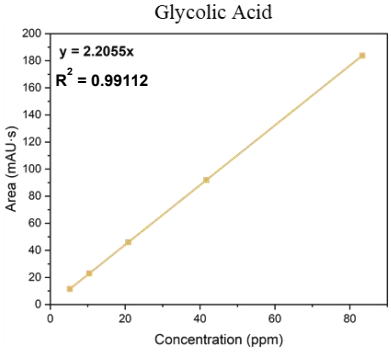
Table S11 High Performance Liquid Chromatography (HPLC) calibration curve

DAD

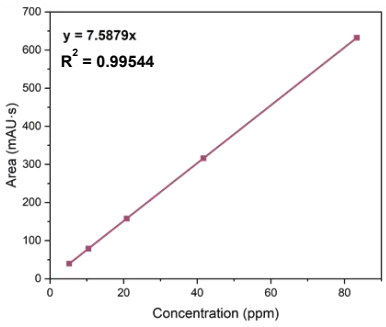
Oxalic Acid



Glycolic Acid

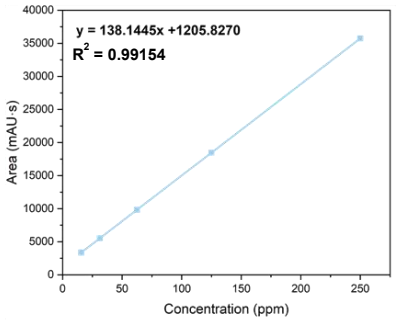


Formic Acid

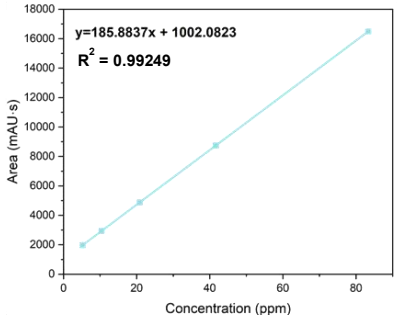


RID

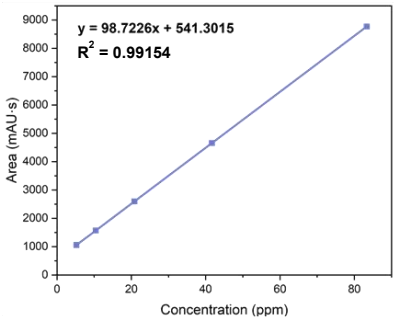
Ethylene Glycol



Methanol



Ethanol



References

[1] D. Zhong, Q. Fang, R. Du, Y. Jin, C. Peng, D. Cheng, T. Li, T. Zhao, S. Zhang, Y. Zheng, Q. Zhao, Y. Sun, J. Li, Angew. Chem. Int. Ed., **2025,** 64, e202501773.

[2] F. Li, Y.C. Li, Z. Wang, J. Li, D.-H. Nam, Y. Lum, M. Luo, X. Wang, A. Ozden, S.-F. Hung, Nat. Catal., **2020,** 3, 75-82.

[3] Gurudayal, J. Bullock, D.F. Srankó, C.M. Towle, Y. Lum, M. Hettick, M.C. Scott, A. Javey, J. Ager, Energy Environ. Sci., **2017,** 10, 2222-2230.

[4] Q. Li, J. Wu, C. Yang, S. Li, C. Long, Z. Zhuang, Q. Li, Z. Guo, X. Huang, Z. Tang, H. Li, D. Wang, Y. Li, J. Am. Chem. Soc., **2025,** 147, 6688-6697.

[5] X. Liu, X. He, D. Xiong, G. Wang, Z. Tu, D. Wu, J. Wang, J. Gu, Z. Chen, ACS Catal., **2024,** 14, 5366-5376.

[6] S. Yue, Z. Zhao, Y. Liu, M. Yang, T. Zhang, F. Li, K. Liu, P. Wang, S. Zhan, Adv. Funct. Mater., **2025,** n/a, 09766.

[7] X. Jiang, P. Wang, Y. Zhang, L. Zhao, Y. Yang, Y. Liu, Chem. Eng. J., **2024,** 502, 157962.

[8] S. Kang, W. Yuan, X. Guo, Y. Zhang, J. Shang, P. Yang, Y. Ma, V. Nicolosi, L. Cai, B. Qiu, Angew. Chem. Int. Ed., **2025,** 64, e202504993.

[9] J. Chang, L. Wang, Z. Hu, S. Zhi, D. Wu, K. Jiang, Z. Gao, Chem. Eng. J., **2025,** 520, 166475.

[10] X. Zheng, Y. Hu, X. Wang, J. Zhu, X. Zhang, T. Sheng, Z. Wu, Angew. Chem. Int. Ed., **2025,** 64, e202415273.

[11] X. Wang, Z. Wang, F.P. García de Arquer, C.-T. Dinh, A. Ozden, Y.C. Li, D.-H. Nam, J. Li, Y.-S. Liu, J. Wicks, Z. Chen, M. Chi, B. Chen, Y. Wang, J. Tam, J.Y. Howe, A. Proppe, P. Todorović, F. Li, T.-T. Zhuang, C.M. Gabardo, A.R. Kirmani, C. McCallum, S.-F. Hung, Y. Lum, M. Luo, Y. Min, A. Xu, C.P. O'Brien, B. Stephen, B. Sun, A.H. Ip, L.J. Richter, S.O. Kelley, D. Sinton, E.H. Sargent, Nat. Energy, **2020,** 5, 478-486.

[12] Z. Gu, H. Shen, Z. Chen, Y. Yang, C. Yang, Y. Ji, Y. Wang, C. Zhu, J. Liu, J. Li, T.-K. Sham, X. Xu, G. Zheng, Joule, **2021,** 5, 429-440.

[13] F. Li, Y.C. Li, Z. Wang, J. Li, D.-H. Nam, Y. Lum, M. Luo, X. Wang, A. Ozden, S.-F. Hung, B. Chen, Y. Wang, J. Wicks, Y. Xu, Y. Li, C.M. Gabardo, C.-T. Dinh, Y. Wang, T.-T. Zhuang, D. Sinton, E.H. Sargent, Nat. Catal., **2020,** 3, 75-82.

[14] X. Wang, Z. Jiang, P. Wang, Z. Chen, T. Sheng, Z. Wu, Y. Xiong, Angew. Chem. Int. Ed., **2023,** 62, e202313646.

[15] J.H. Lee, W. Jang, H. Lee, D. Oh, W.Y. Noh, K.Y. Kim, J. Kim, H. Kim, K. An, M.G. Kim, Y. Kwon, J.S. Lee, S. Cho, Nano Lett., **2024,** 24, 9322-9330.

[16] M. Serafini, F. Mariani, A. Fasolini, E.T. Brandi, E. Scavetta, F. Basile, D. Tonelli, Adv. Funct. Mater., **2023,** 33, 2300345.

[17] Y.N. Xu, W. Li, H.Q. Fu, X.Y. Zhang, J.Y. Zhao, X. Wu, H.Y. Yuan, M. Zhu, S. Dai, P.F. Liu, H.G. Yang, Angew. Chem. Int. Ed., **2023,** 62, e202217296.

[18] Q. Fan, X. Zhang, X. Ge, L. Bai, D. He, Y. Qu, C. Kong, J. Bi, D. Ding, Y. Cao, X. Duan, J. Wang, J. Yang, Y. Wu, Adv. Energy Mater., **2021,** 11, 2101424.

[19] G. Miao, L. Liu, X. An, X. Wu, Chin. J. Chem. Eng., **2023,** 64, 156-167.

[20] X. Ma, T. Liu, E. Liu, Y. Zhang, Molecular Catalysis, **2023,** 535, 112876.

[21] K. Iwase, T. Hirano, I. Honma, ChemSusChem, **2022,** 15, e202102340.

[22] X. Zhang, C. Liu, Y. Zhao, L. Li, Y. Chen, F. Raziq, L. Qiao, S.-X. Guo, C. Wang, G.G. Wallace, A.M. Bond, J. Zhang, Appl. Catal., B, **2021,** 291, 120030.

[23] Y. Wang, H. Xu, Y. Liu, J. Jang, X. Qiu, E.P. Delmo, Q. Zhao, P. Gao, M. Shao, Angew. Chem. Int. Ed., **2024,** 63, e202313858.

[24] U.T. Dieu Thuy, T.N. Huan, S. Zanna, K. Wilson, A.F. Lee, N.-D. Le, J. Mensah, V.D.B.C. Dasireddy, N.Q. Liem, RSC Advances, **2024,** 14, 3489-3497.

[25] F.M. Yap, J.Y. Loh, S. Yuan, X. Zeng, W.-J. Ong, Adv. Funct. Mater., **2024,** 2407605.

[26] J.R.C. Junqueira, P.B. O'Mara, P. Wilde, S. Dieckhöfer, T.M. Benedetti, C. Andronescu, R.D. Tilley, J.J. Gooding, W. Schuhmann, ChemElectroChem, **2021,** 8, 4848-4853.

[27] S. Lee, G. Park, J. Lee, ACS Catal., **2017,** 7, 8594-8604.

[28] Q. Zhu, X. Sun, D. Yang, J. Ma, X. Kang, L. Zheng, J. Zhang, Z. Wu, B. Han, Nat. Commun., **2019,** 10, 3851.

[29] S. Zhang, S. Zhao, D. Qu, X. Liu, Y. Wu, Y. Chen, W. Huang, Small, **2021,** 17, 2102293.

[30] F.A. Rollier, V. Muravev, N. Kosinov, T. Wissink, D. Anastasiadou, B. Ligt, L. Barthe, M. Costa Figueiredo, E.J.M. Hensen, J. Mater. Chem. A, **2025,** 13, 2285-2300.

[31] Q. Bie, H. Yin, Y. Wang, H. Su, Y. Peng, J. Li, Chinese J. Catal., **2024,** 57, 96-104.

[32] D. Fan, S. Zhang, Y. Li, H. Bin, R. Li, Y. Li, M. An, P. Yang, J. Zhang, J. Colloid Interface Sci., **2024,** 662, 786-795.

[33] B. Huang, F. Zhao, J. Fu, L. Zheng, J. Zhang, D. Zhao, Chem. Commun., **2025**.

[34] S. Behera, S. Dinda, R. Saha, B. Mondal, ACS Catal., **2023,** 13, 469-474.

[35] T. Ren, Z. Yu, H. Yu, K. Deng, Z. Wang, X. Li, H. Wang, L. Wang, Y. Xu, ACS Nano., **2023,** 17, 12422-12432.

[36] H. Zhang, Z. Liu, H. Li, Z. Fu, G. Zhang, H. Zhang, G. Wang, Y. Zhang, J. Mater. Chem. A, **2024,** 12, 15984-15995.

[37] S.K. Kilaparthi, A. Addad, A. Barras, S. Szunerits, R. Boukherroub, J. Mater. Chem. A, **2023,** 11, 26075-26085.

[38] X. Lu, Y. Guo, H. Fu, J. Song, C. Liang, H. Jiang, Z. Wang, Y. Liu, H. Cheng, Z. Zheng, Y. Wu, P. Wang, B. Huang, Chem. Eng. J., **2025,** 506, 159810.

[39] D. Du, P. Liu, Z. Teng, T. Chen, J. Zhu, B. Shao, J. Luo, ACS Catal., **2025,** 15, 3038-3045.

[40] J. Wang, X. Li, M. Wang, T. Zhang, X. Chai, J. Lu, T. Wang, Y. Zhao, D. Ma, ACS Catal., **2022,** 12, 6722-6728.

[41] G. Zhao, J. Lin, M. Lu, L. Li, P. Xu, X. Liu, L. Chen, Nat. Commun., **2024,** 15, 8463.

[42] J. Chen, F. Zhang, M. Kuang, L. Wang, H. Wang, W. Li, J. Yang, Proc. Natl. Acad. Sci. USA, **2024,** 121, e2318853121.

[43] Y. Zhou, T. Tian, S. Jiang, R. Shen, H. Yu, Z. Wang, H. Wang, L. Wang, K. Deng, Adv. Funct. Mater., **2025,** n/a, e11835.

[44] M. Jiang, Y. Yang, Y. Wang, Y. Wang, M. Ratova, W. Dai, D. Wu, Chem. Eng. Sci., **2025,** 317, 122101.